

**SYNTHESIS AND CHARACTERIZATION OF  
TITANIUM DIOXIDE PARTICLES BY DIRECT  
HEATING TECHNIQUE FOR  
PHOTODEGRADATION OF METHYLENE  
BLUE SOLUTION**

**NG GUAN SHENG**

**UNIVERSITI SAINS MALAYSIA**

**2022**

SCHOOL OF MATERIALS AND MINERAL RESOURCES ENGINEERING  
UNIVERSITI SAINS MALAYSIA

SYNTHESIS AND CHARACTERIZATION OF TITANIUM DIOXIDE PARTICLES  
BY DIRECT HEATING TECHNIQUE FOR PHOTODEGRADATION OF  
METHYLENE BLUE SOLUTION

By

NG GUAN SHENG

Supervisor: Assoc. Prof. Ts. Ir. Dr. Pung Swee Yong

Dissertation submitted in partial fulfillment  
of the requirements for the degree of Bachelor of Engineering with Honours  
(Materials Engineering)

Universiti Sains Malaysia

AUGUST 2022

SCHOOL OF MATERIALS AND MINERAL RESOURCES ENGINEERING  
UNIVERSITI SAINS MALAYSIA

SYNTHESIS AND CHARACTERIZATION OF TITANIUM DIOXIDE PARTICLES  
BY DIRECT HEATING TECHNIQUE FOR PHOTODEGRADATION OF  
METHYLENE BLUE SOLUTION

By

NG GUAN SHENG

Supervisor: Assoc. Prof. Ts. Ir. Dr. Pung Swee Yong

Dissertation submitted in partial fulfillment  
of the requirements for the degree of Bachelor of Engineering with Honours  
(Materials Engineering)

Universiti Sains Malaysia

AUGUST 2022

## DECLARATION

I hereby declare that I have conducted, completed the research work and written the dissertation entitled '**Synthesis and Characterization of Titanium Dioxide Particles by Direct Heating Technique for Photodegradation of Methylene Blue Solution**'. I also declare that it has not been previously submitted for the award of any degree and diploma or other similar title of this for any other examining body or University.

Name of Student: Ng Guan Sheng

Signature:

Date: 12 August 2022

Witness by

Supervisor: Assoc. Prof. Ts. Ir. Dr. Pung

Signature:

Swee Yong

Date: 12 August 2022

## **ACKNOWLEDGEMENT**

First of all, I would like to express my gratitude to University of Science Malaysia and School of Materials and Mineral Resources Engineering for providing me this opportunity to complete this research. I am grateful that School of Materials and Mineral Resources Engineering provided me sufficient equipment and workspace to complete this research. I would like to give a special gratitude to my supervisor, Assoc. Prof. Ts. Ir. Dr. Pung Swee Yong for giving me valuable advice, guiding me patience in answering all my questions, and guiding me through the process. His guidance, motivation, and support really help me to complete my research and writing my thesis.

Besides my supervisor, I would like to take this opportunity to thank you all the technicians of School of Materials and Mineral Resources Engineering who have directly and indirectly involved in my research especially Mr Sharul, Miss Mahani, Mr Syafiq, Mr Zaini, Mr Azrul, Mr Azam, and Mr Helmi.

Finally, I would like to thank my beloved parent, Ng Gim Fatt and Wong Kim Fong for their unending emotional, moral, spiritual, and financial support. Besides, I would like to acknowledge all my friends especially Kok Kai Lin and Liong Kai Ming who share their thoughts, knowledges, and ideas with me. This project would not have been completed without those who directly or indirectly helping me throughout the research.

## TABLE OF CONTENT

<b>DECLARATION .....</b>	<b>i</b>
<b>ACKNOWLEDGEMENT.....</b>	<b>ii</b>
<b>TABLE OF CONTENT.....</b>	<b>iii</b>
<b>LIST OF TABLES .....</b>	<b>vi</b>
<b>LIST OF FIGURES .....</b>	<b>viii</b>
<b>LIST OF ABBREVIATIONS .....</b>	<b>xiii</b>
<b>LIST OF SYMBOLS .....</b>	<b>xiv</b>
<b>ABSTRACT .....</b>	<b>xv</b>
<b>ABSTRACT.....</b>	<b>xvi</b>
<b>CHAPTER 1 INTRODUCTION.....</b>	<b>1</b>
1.1    Background of study .....	1
1.2    Problem statement.....	9
1.3    Research objectives.....	11
1.4    Scope of study.....	11
1.5    Thesis outline .....	12
<b>CHAPTER 2 LITERATURE REVIEW.....</b>	<b>13</b>
2.1    Introduction.....	13
2.2    Titanium Dioxide (TiO <sub>2</sub> ) .....	13
2.2.1    TiO <sub>2</sub> for photocatalyst application .....	15
2.3    Synthesis route of TiO <sub>2</sub> nanomaterials .....	17
2.3.1    Hydrothermal method .....	17
2.3.2    Template-assisted method.....	19
2.3.3    Sol-gel method.....	21
2.3.4    Electrochemical anodization .....	23
2.3.5    Microwave-assisted method .....	25

2.3.6	Chemical vapour deposition (CVD) .....	27
2.3.7	Direct Heating technique .....	28
2.3.8	Advantages and disadvantages of various synthesis methods .....	29
2.4	Photocatalytic oxidation of methylene blue solution by TiO <sub>2</sub> nanoparticles..	33
2.4.1	Methylene blue .....	33
2.4.2	Degradation mechanism of methylene blue by TiO <sub>2</sub> .....	35
2.5	Scavenger test .....	40
<b>CHAPTER 3 RESEARCH METHODOLOGY.....</b>		<b>42</b>
3.1	Introduction.....	42
3.2	Project Flow Chart .....	42
3.3	Materials and Equipment .....	43
3.4	Synthesis of TiO <sub>2</sub> particles grown on the Kanthal wire by Direct Heating technique .....	45
3.4.1	Experimental procedure .....	45
3.4.2	Experimental design .....	47
3.4.2.1	Different period of heating duration .....	48
3.4.2.2	Different heating power .....	48
3.5	Characterization techniques .....	49
3.5.1	X-ray Powder Diffraction (XRD).....	49
3.5.2	Field emission scanning electron microscopy (FESEM).....	51
3.5.3	Transmission electron microscopy (TEM) .....	52
3.5.4	Ultraviolet–visible (UV-Vis) spectroscopy .....	54
3.5.4.1	TiO <sub>2</sub> nanoparticles absorbance .....	55
3.5.5	Fourier Transformed Infrared (FTIR) spectroscopy .....	55
3.6	Photocatalytic oxidation of methylene blue solution by TiO <sub>2</sub> particles .....	57
3.7	Scavenger test .....	59
<b>CHAPTER 4 RESULTS AND DISCUSSION.....</b>		<b>60</b>

4.1	Introduction.....	60
4.2	Synthesis and characterization of TiO <sub>2</sub> particles deposited on Kanthal wire and TiO <sub>2</sub> powders (by-products).....	60
4.2.1	Effect of heating duration .....	61
4.2.1.1	Crystal phase and phase content identification by XRD .....	61
4.2.1.2	Identification of Ti-O bond by FTIR .....	66
4.2.1.3	Morphology and particle size characterization by SEM.....	67
4.2.1.4	Methylene blue removal by TiO <sub>2</sub> particles deposited on Kanthal wires using different synthesis durations .....	71
4.2.2	Effect of heating power.....	77
4.2.2.1	Crystal phase and phase content identification by XRD .....	77
4.2.2.2	Identification of Ti-O bond by using FTIR .....	79
4.2.2.3	Morphology and particle size characterization by SEM.....	80
4.2.2.4	Methylene blue removal by TiO <sub>2</sub> particles deposited on Kanthal wires using different heating powers.....	84
4.2.3	A detail analyses on the TiO <sub>2</sub> particles grown on Kanthal wires using optimized synthesis parameters by Direct Heating technique.....	90
4.2.4	Growth mechanism of TiO <sub>2</sub> particles on Kanthal wires using Direct Heating technique.....	92
4.3	Photocatalytic performances of TiO <sub>2</sub> particles (by-product) produced using optimum synthesis condition by Direct Heating technique with the commercial TiO <sub>2</sub> particles .....	94
<b>CHAPTER 5 CONCLUSIONS AND RECOMMENDATIONS .....</b>		<b>102</b>
5.1	Conclusions.....	102
5.2	Recommendations.....	103
<b>REFERENCES.....</b>		<b>104</b>
<b>APPENDICES.....</b>		<b>114</b>



## LIST OF TABLES

Table 1.1: A comparison of synthesis duration, equipment cost, energy used and operational cost for the synthesis of TiO <sub>2</sub> particles .....	10
Table 2.1: The advantages and disadvantages of various methods for synthesis of TiO <sub>2</sub> nanostructures .....	30
Table 2.3: The reactive species and their responsible scavenger agent.....	41
Table 3.1: Lists of chemicals and materials used in this project .....	43
Table 3.2: Lists of equipment used in this project .....	44
Table 3.3: Effect of heating duration on the growth of TiO <sub>2</sub> particles using DH technique .....	48
Table 3.4: Effect of heating power on the growth of TiO <sub>2</sub> particles using DH technique .....	48
Table 3.5: Chemicals used in scavenger tests .....	59
Table 4.1: The amount of TiO <sub>2</sub> crystal phases (by-products) produced at different heating duration using Direct Heating technique .....	65
Table 4.2: The size of TiO <sub>2</sub> nanoparticles deposited on Kanthal wires at different heating duration (n = 30) .....	69
Table 4.3: Photodegradation efficiency of samples at different synthesis duration .....	73
Table 4.4: Kinetic parameters for the degradation of MB dye by TiO <sub>2</sub> particles grown on Kanthal wires synthesized at different synthesis duration .....	77
Table 4.5: The crystal phase content of TiO <sub>2</sub> particles (by-products) at different heating power using Direct Heating technique.....	79
Table 4.6: The size of TiO <sub>2</sub> nanoparticles deposited on Kanthal wires at different heating power (n = 30).....	83
Table 4.7: Photodegradation efficiency of samples at different heating powers .....	86

Table 4.8: Kinetic parameters for the degradation of MB dye by TiO <sub>2</sub> particles grown on Kanthal wires synthesized at different heating power .....	88
Table 4.9: Photodegradation efficiencies of commercial TiO <sub>2</sub> particles and TiO <sub>2</sub> particles (by product) in removal of MB under UV irradiation .....	96
Table 4.10: Photodegradation efficiency of TiO <sub>2</sub> particles (by product) with the addition of different scavenger agent.....	101

## LIST OF FIGURES

Figure 1.1: Classification of dyes (Bharagava and Bhimrao, 2018).....	2
Figure 1.2: Sources and pathways of dyes to the environment (Dutta <i>et al.</i> , 2021) .....	3
Figure 1.3: River water quality trend in Malaysia from year 2008-2019 (Rani <i>et al.</i> , 2021). .....	4
Figure 1.4: Major types of Advanced Oxidation Processes (Biń and Sobera-Madej, 2012) .....	6
Figure 1.5: Photocatalytic degradation mechanism (Mull, Möhlmann and Wilke, 2017)	8
Figure 2.1: Crystal structure of crystalline forms of rutile, anatase and brookite TiO <sub>2</sub> NPs (Baranowska-Wójcik <i>et al.</i> , 2020) .....	14
Figure 2.2: Teflon lined stainless steel autoclaves with inner components (Kafle, 2020) .....	18
Figure 2.3: TEM image of TiO <sub>2</sub> nanoparticles after hydrothermal treatment of HNO <sub>3</sub> peptized gel at (a) 210 °C and (b) 270 °C (Rehan, Lai and Kale, 2011) .....	19
Figure 2.4: SEM image of commercial AAO membrane (top view) (Pradel and Fukata, 2022) .....	20
Figure 2.5: Working principle of AAO template-assisted electrodeposition method (Pradel and Fukata, 2022) .....	20
Figure 2.6: Schematic diagram of different stages in sol-gel process (Bokov <i>et al.</i> , 2021) .....	22
Figure 2.7: TEM micrographs of TiO <sub>2</sub> nanoparticles formed by sol-gel process at resolution (a) 200 nm (b) 100 nm (c) 50 nm (d) SAED pattern (Dubey, Krishnamurthy and Singh, 2019) .....	23
Figure 2.8: Experiment setup of electrochemical anodization for synthesis of titania nanotube array (TNA) (Bhattacharyya <i>et al.</i> , 2016) .....	24

Figure 2.9: SEM micrograph of TiO <sub>2</sub> nanotube top view and side view synthesized by electrochemical anodization (Bhattacharyya <i>et al.</i> , 2016).....	25
Figure 2.10: Synthesis of TiO <sub>2</sub> nanoparticles and TiO <sub>2</sub> nanoparticles with gold (Au) by microwave-assisted method (Machut <i>et al.</i> , 2020) .....	26
Figure 2.11: Typical set up for CVD technique. (Madhuri, 2020) .....	27
Figure 2.12: (a) Molecular structure (Aguiar <i>et al.</i> , 2014) and (b) intrinsic absorbance (Whang <i>et al.</i> , 2009) of MB.....	33
Figure 2.13: MB as a redox-cycling substrate for various reducing and oxidizing substances. (Oz <i>et al.</i> , 2011) .....	35
Figure 2.14: Electronic reorganization during the passage of MB adsorbed to the sulfoxide form. (Houas <i>et al.</i> , 2001).....	37
Figure 2.15: MB photodegradation mechanism by UV/TiO <sub>2</sub> (Houas <i>et al.</i> , 2001) .....	39
Figure 3.1: Project Flow Chart .....	42
Figure 3.2: Kanthal wire (substrate material) with 8 turns and 20 mm in length .....	45
Figure 3.3: Experiment setup for direct heating technique.....	47
Figure 3.4: Schematic diagram of direct heating technique .....	47
Figure 3.5: Schematic diagram of incident plane wave that fulfil Bragg's Law (Pederson, 2019) .....	50
Figure 3.6: Working principle of FESEM (Semnani, 2017).....	52
Figure 3.7: Working principle of TEM (Senthil Kumar, Grace Pavithra and Naushad, 2019) .....	53
Figure 3.8: Working principle of UV-Vis spectroscopy (Tom, 2021) .....	54
Figure 3.9: Schematic diagram of FTIR spectrometer (Titus, James Jebaseelan Samuel and Roopan, 2019).....	56

Figure 4.1: Bare Kanthal wire with shiny surface (left), and Kanthal wire covered with a white layer (right) after direct heating process. ....	61
Figure 4.2: Schematic diagram of TiO <sub>2</sub> particles that grown on Kanthal wire .....	62
Figure 4.3: XRD patterns of Kanthal wire and particles deposited on Kanthal wire (60 W, 15 min) using DH technique .....	63
Figure 4.4: Schematic diagram of TiO <sub>2</sub> (by-product) after DH process.....	64
Figure 4.5: XRD patterns of TiO <sub>2</sub> particles produced at different heating duration using DH technique .....	64
Figure 4.6: FTIR spectrum of TiO <sub>2</sub> particles with different synthesis duration .....	67
Figure 4.7: SEM images of TiO <sub>2</sub> deposited on Kanthal wires for 60 W at (a) 0 (bare Kanthal wire), (b) 15, (c) 30, (d) 45 and (e) 60 min at magnification of 500X.....	68
Figure 4.8: FESEM images of TiO <sub>2</sub> particles deposited on Kanthal wires for 60 W at (a) 0 (bare Kanthal wire), (b) 15, (c) 30, (d) 45 and (e) 60 min at magnification of 30kX..	70
Figure 4.9: The size distribution of TiO <sub>2</sub> particles deposited on Kanthal wires in pH 1 solution for 60 W at (a) 15, (b) 30, (c) 45 and (d) 60 min. ....	71
Figure 4.10: UV-Vis absorbance spectra of MB solution degraded by TiO <sub>2</sub> particles on Kanthal wires prepared at (a) 0 (bare Kanthal wire), (b) 15, (c) 30, (d) 45 and (e) 60 min .....	72
Figure 4.11: Photodegradation efficiency of MB dye degraded by TiO <sub>2</sub> particles synthesized using different duration (a) as a function of UV light irradiation time, and (b) at 90 min of UV light irradiation .....	74
Figure 4.12: Kinetic plots of (a) Pseudo-zero-order, (b) Pseudo-first-order, (c) Pseudo-second-order; and (d) rate constants for photodegradation of MB dye by TiO <sub>2</sub> particles grown on Kanthal wires synthesized at different heating duration.....	76
Figure 4.13: XRD patterns of TiO <sub>2</sub> particles produced at different heating powers with 15 heating time and pH 1 using DH technique .....	78

Figure 4.14: FTIR spectrum of TiO <sub>2</sub> particles with different heating power. ....	80
Figure 4.15: SEM images of TiO <sub>2</sub> deposited on Kanthal wires in pH 1 solution for 15 min at (a) 0, (b) 30, (c) 40, (d) 50, (e) 60 and (f) 70 W at magnification of 500X. ....	81
Figure 4.16: FESEM images of TiO <sub>2</sub> deposited on Kanthal wires in pH 1 solution for 15 min at (a) 0, (b) 30, (c) 40, (d) 50, (e) 60 and (f) 70 W at magnification of 30kX. ....	82
Figure 4.17: The size distribution of TiO <sub>2</sub> particles deposited on Kanthal wires in pH 1 solution for 15 min at different heating power. ....	84
Figure 4.18: UV-Vis absorbance spectra of MB solution degraded by TiO <sub>2</sub> particles on Kanthal wires prepared at (a) 0 (bare Kanthal wire), (b) 30, (c) 40, (d) 50 and (e) 60, (f) 70 W. ....	85
Figure 4.19: Photodegradation efficiency of MB dye degraded by TiO <sub>2</sub> particles with different heating powers (a) as a function of UV light irradiation time, and (b) at 90 min of UV light irradiation ....	87
Figure 4.20: Kinetic plots of (a) Pseudo-zero-order, (b) Pseudo-first-order, (c) Pseudo-second-order; and (d) rate constants for photodegradation of MB dye by TiO <sub>2</sub> particles grown on Kanthal wires synthesized at different heating power. ....	89
Figure 4.21: TEM images of TiO <sub>2</sub> particles deposited on Kanthal wire at the magnification of 490 kX. ....	90
Figure 4.22: TEM images of optimized TiO <sub>2</sub> particles deposited on Kanthal wire at the magnification of (a) 43kX, (b) 97kX, (c) 195kX; HRTEM images showing the presence of anatase phase and brookite phase TiO <sub>2</sub> ....	91
Figure 4.23: The EDX analysis of TiO <sub>2</sub> particles deposited on Kanthal wire using optimum synthesis condition by Direct Heating technique. ....	92
Figure 4.24: UV-Vis absorbance spectra of MB solution degraded by (a) commercial TiO <sub>2</sub> particles and (b) TiO <sub>2</sub> particles (by product) produced by optimum synthesis condition using DH technique. ....	95

Figure 4.25: Photodegradation efficiency of MB dye degraded by commercial TiO<sub>2</sub> particles and TiO<sub>2</sub> particles (by product) produced by optimum synthesis condition using Direct Heating technique (a) as a function of UV light irradiation time, and (b) at 90 min of UV light irradiation ..... 97

Figure 4.26: UV-Vis absorbance spectra of MB solution degraded by TiO<sub>2</sub> particles (by product) with (a) no addition of scavenger agent, addition of (b) H<sub>2</sub>O<sub>2</sub>, (c) EDTA, (d) IPA and (e) P-BQ scavenger agent ..... 98

Figure 4.27: Photodegradation efficiency of MB dye degraded by TiO<sub>2</sub> particles (by product) with the addition of different scavenger agents (a) as a function of UV light irradiation time, and (b) at 90 min of UV light irradiation ..... 100

## LIST OF ABBREVIATIONS

AAO	Anodized Alumina Membrane
AC	Alternating Current
ANOVA	Analysis of Variance
AOPs	Advance Oxidation Process
CVD	Chemical Vapour Deposition
DH	Direct Heating
DOE	Department of Environment
DSSC	Dye-sensitized Solar Cell
EDTA	Ethylenediaminetetraacetic acid
EDXRD	Energy Dispersive X-ray Diffraction
FESEM	Field Emission Scanning Electron Microscopy
FTIR	Fourier Transformed Infrared
IPA	Isopropanol
LIBs	Lithium-ion Batteries
MB	MB
NADPH	Nicotinamide Adenine Dinucleotide Phosphate
P-BQ	Para-Benzoquinone
PAHs	Poly Aromatic Hydrocarbon
PCA	Photocatalytic Activity
PCBs	Polychlorinated Biphenyls
PECVD	Plasma-enhance CVD
PVP	Polyvinylpyrrolidone
TBA	Tetrabutylammonium Hydroxide
TEM	Transmission Electron Microscopy
TM	Tabletop Microscope
TNA	Titania Nanotube Array
TTIP	Titanium Tetra-isopropoxide
UV-Vis	Ultraviolet-visible
WQI	Water Quality Index
WWTPs	Wastewater treatment plants
XRD	X-ray Powder Diffraction



## LIST OF SYMBOLS

$\lambda$	Wavelength
$\theta$	Angle
$\Omega\cdot\text{cm}$	Electrical Resistivity
$\mu\text{m}$	Micrometer
$^{\circ}\text{C}$	Degree Celcius
atm	Atmospheric Pressure
cm	Centimeter
$E_{\text{B}}$	Binding Energy
$E_{\text{K}}$	Kinetic Energy
eV	Band Gap Energy
g/mol	Gram per mole (Molar Mass)
GHz	Gigahertz
hr	Hour
K	Kelvin
kV	Kilovolt
kW	Kilowatt
kWh	Kilowatt hour
mg	Milligram
min	Minute
ml	Millileter
mM	Concentration
mm	Millimeter
ng/L	Nanograms per Liter
nm	Nanometer
RM	Ringgit Malaysia
rpm	Revolutions per Minute
W	Watt
wt%	Weight Percent
$\alpha$	Alpha
$R^2$	Correlation Coefficient

## ABSTRACT

Pewarna digunakan secara meluas dalam industri tekstil dan ia akan membebaskan air sisa dengan jumlah yang besar dan pewarna ini membahayakan manusia dan alam sekitar. Proses pengoksidaan lanjutan (AOP) berdasarkan fotomangkin  $\text{TiO}_2$  heterogen adalah salah satu teknologi yang telah terbukti berjaya untuk rawatan efluen. Matlamat kerja penyelidikan ini adalah untuk mensintesis partikel  $\text{TiO}_2$  pada dawai Kanthal dengan menggunakan teknik Pemanasan Terus dengan tempoh pemanasan dan kuasa pemanasan yang berbeza. Partikel  $\text{TiO}_2$  yang tumbuh pada wayar Kanthal dan produk sampingannya diukur dari segi prestasi struktur, optik dan prestasi fotomangkinnya. Larutan prekursor disediakan dengan mencampurkan 5 ml titanium tetraisopropoxide (TTIP) dengan 15 ml isopropanol. Larutan 250 ml air suling dicampur dengan larutan asid hidroklorik (HCl) untuk mencapai pH 1. Kemudian, 2 titik hidrogen peroksida ( $\text{H}_2\text{O}_2$ ) telah ditambah kepada larutan campuran untuk menggalakkan pembentukan  $\text{TiO}_2$ . Pengatur AC dihidupkan selama 60 W dan 30 minit, kemudian gegelung wayar dibilas dengan air suling, dikeringkan di udara dan dicirikan oleh pelbagai teknik pencirian. Keadaan sintesis optimum untuk Pemanasan Terus ialah tempoh pemanasan selama 15 minit dan kuasa pemanasan 60 W.  $\text{TiO}_2$  termendap optimum mengandungi campuran anatase (82.7%) dan brookite (17.3%), saiz partikel purata bagi  $167.36 \pm 15.37$  nm, liputan permukaan zarah  $\text{TiO}_2$  pada Kawat Kanthal adalah baik, dengan aglomerasi minimum, dan kecekapan fotodegradasi tertinggi (43.7%). TEM menunjukkan kehadiran nanorod dan nanopartikel (dengan saiz  $5.766 \pm 1.302$  nm), dan spektrum EDX seterusnya mengesahkan kehadiran  $\text{TiO}_2$  yang dienap pada wayar Kanthal. Partikel  $\text{TiO}_2$  hasil sampingan mempunyai kecekapan fotodegradasi yang lebih tinggi (36.5%) daripada partikel  $\text{TiO}_2$  komersial (16.3%). Selain itu, hasil sampingan digunakan untuk ujian pemulung. Spesies reaktif utama dalam degradasi metilena biru ialah  $\bullet\text{OH}$ .

## ABSTRACT

Dyes are extensively used in textile industry and it will release large amount of dye-containing wastewater which is hazardous to human and environment. Advanced oxidation process (AOPs) based on heterogeneous  $\text{TiO}_2$  photocatalyst is one such technology that has proven successful for effluent treatment. The aim of this research work is to synthesize  $\text{TiO}_2$  particles on Kanthal wire by using Direct Heating technique with different heating duration and heating power.  $\text{TiO}_2$  particles that grown on Kanthal wire and its by product was measured in terms of its structural, optical and photocatalytic performances. The precursor solution was prepared by mixing 5 ml of titanium tetraisopropoxide (TTIP) with 15 ml isopropanol. A 250 ml solution of distilled water mixed with hydrochloric acid solution (HCl) to reach pH 1. Then, 2 drops of hydrogen peroxide ( $\text{H}_2\text{O}_2$ ) were added to the mixture solution to promote the formation of  $\text{TiO}_2$ . The Kanthal coil was immersed into the mixture solution. The AC regulator was switched on for 60 W and 30 minutes, then the wire coil was rinsed with distilled water, air dried and was characterized by various characterization techniques. The optimum synthesis condition for Direct Heating was heating duration of 15 min and heating power of 60 W. Optimum deposited  $\text{TiO}_2$  contained mixture of anatase (82.7%) and brookite (17.3%), average particle size of  $167.36 \pm 15.37$  nm, surface coverage of  $\text{TiO}_2$  particles on Kanthal wire was good, with minimum agglomeration, and the highest photodegradation efficiency (43.7%). TEM shows the presence of aligned nanorods and nanoparticles (with the size of  $5.766 \pm 1.302$  nm), and EDX spectrum further confirms the presence of  $\text{TiO}_2$  deposited on Kanthal wire. The by-product  $\text{TiO}_2$  particles has a higher photodegradation efficiency (36.5 %) than the commercial  $\text{TiO}_2$  particles (16.3 %). Besides, by-product  $\text{TiO}_2$  particles was used for scavenger test. The major reactive species in the degradation of MB was  $\bullet\text{OH}$ .

## CHAPTER 1 INTRODUCTION

### 1.1 Background of study

In order to maintain a healthy ecosystem, high quality surface water and safe drinking water is an essential. Water pollution by human had make the water unsafe for human use and disrupts the ecosystem or the aquatic ecosystems. Nowadays, water pollution is the major problem in the global context and there are many water pollutants such as dyes (Upendar, Dutta and Adhikari, 2017), pesticides (Hussain and Asi, 2018), lead (Seema Tiwari, I.P. Tripathi, 2013), arsenic (Shaji *et al.*, 2021), polychlorinated biphenyls (PCBs) (Cui *et al.*, 2020) and poly aromatic hydrocarbons (PAHs) (Zhang *et al.*, 2019), which are known as “conventional priority pollutants”.

Dyes are one of the most serious pollutants in the world. Dyes are extensively used in numerous industries for examples in textile, rubber, paper, food and plastics. The effluents from these industries are in coloured form. Discharge of untreated waste or pollutants into the water systems will lead to severe pollution to the aquatic life and environment. Among all the industries, textile industry is one of the largest producers of the liquid effluent pollutants as huge amount of water is used in the dyeing process (Upendar, Dutta and Adhikari, 2017).

Generally, dyes can be classified into 2 types which are natural dyes and synthetic dyes as shown in Figure 1.1. Synthetic dyes are normally toxic and harmful to the mankind and environment as well (Munir *et al.*, 2020). Methylene Blue (MB), which is the focus of this project, is a representative of synthetic, water-soluble azo dye. It can form quaternary ammonium cations in aqueous solution, and it also has a high chroma which can cause serious environmental pollution. It is an odourless dark green crystals or crystalline powder with a bronze luster and become blue when dissolved in water (Bharagava and Bhimrao, 2018).

There are plenty of ways the dye effluents can get into the environment and Figure 1.2 shows the sources, and pathways of dyes being discharged in the environment. The major sources of dye effluents to the environment are from industries which include pharmaceutical industries, textile industries, paints and varnishing industries, food industries, and leather industries. Besides, the minor sources of dye effluents are wastewater treatment plant and household. During the sewage treatment, the dyes are usually not quantitatively removes as they can escape degradation in waste treatment plants and remain in the effluents that are able to get into the surface and groundwater (Dutta *et al.*, 2021).

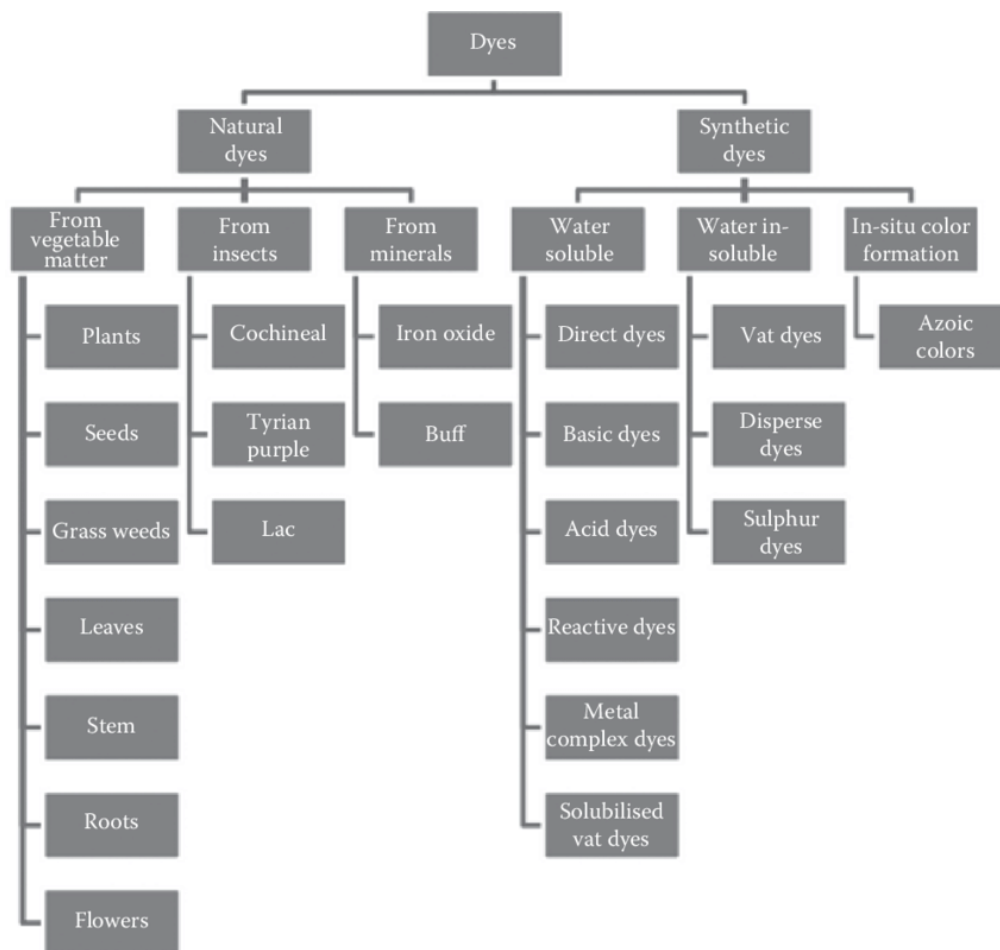


Figure 1.1: Classification of dyes (Bharagava and Bhimrao, 2018)

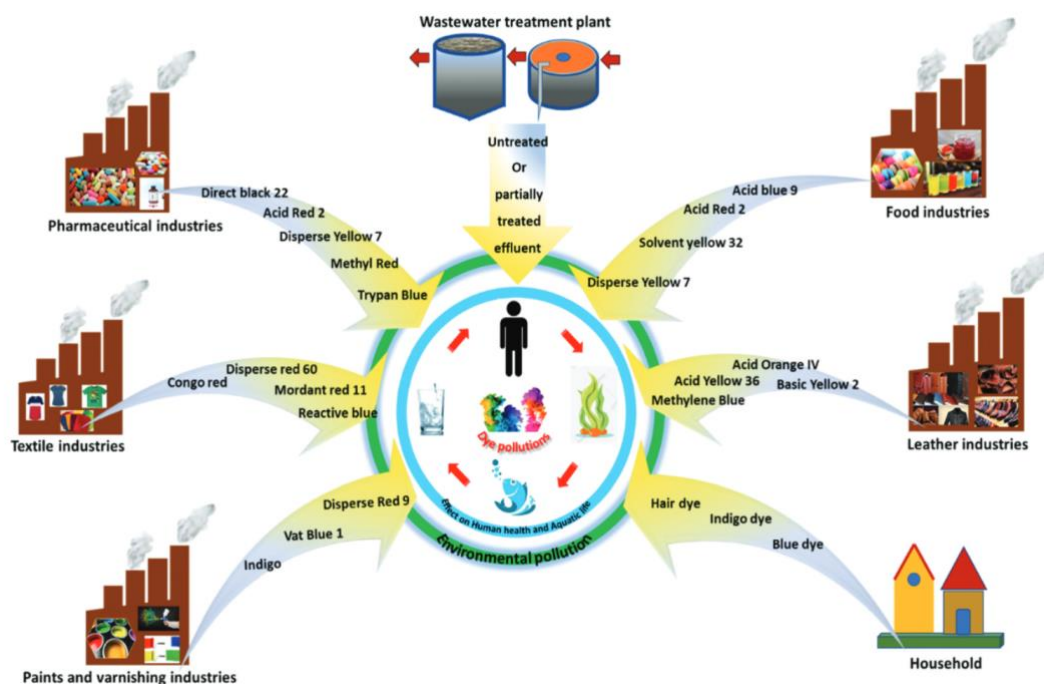


Figure 1.2: Sources and pathways of dyes to the environment (Dutta *et al.*, 2021)

Dyes are extensively used in textile industry of Asia countries and this industry plays a major role in the economy of some Asia countries. For example, India is the second largest exporter of dyestuffs which is after China (also Asia country). According to recent investigations, there are a total of  $7 \times 10^5$  tons of dyestuff is manufactured yearly and is still increasing. It is estimated that about 12% to 14% of dye effluents will be discarded to the environment without proper treatment. The release of the dyes to the environment is because not all dyes will bind to the fabric during the dyeing processes, and they can be losses in wastewater and contaminate the surface and ground waters. It is estimated that globally 280000 tons of textile dyes are discharged as effluent and the deterioration of the aquatic environment by dye-containing effluents will affect the eco-balance of the aquatic flora and fauna. This is because the rivers and sea water that contain the dyes will reduce the light penetration and decreases the amount of dissolved oxygen which affect the photosynthesis of aquatic flora, thereby reducing the food source of aquatic animals (Pereira and Alves, 2012).

In Malaysia, batik which is the traditional craftsmanship of textile has contributed major parts of the textile industry. Batik is considered as a national heritage art and is the pride of Malaysia. Traditional batik industry is usually cultivated by small and medium scale industry nearby the river, and they usually lack awareness about the toxicity of dye and without proper waste management system. Process of making batik will produce large amount of wastewater with dye (especially in colouring process), neglecting or without proper treatment of the effluent will lead to high amount of dyes will be release to the aquatic system (Sajab *et al.*, 2019). Based on Water Quality Index (WQI) classified by the Department of Environment (DOE) Malaysia, many of the rivers in Malaysia are classified as Class II, yellow colour (need conventional water treatment) and Class III, red colour (need extensive water treatment). This is supported by Figure 1.3 which the river water quality trend in Malaysia from year 2008 to 2019. Based on year 2019, the river water quality was assessed based on 672 rivers in Malaysia and 408 (61%) shown clean water quality, but 205 rivers (30%) were slightly polluted, and 59 rivers (9%) were polluted (Rani *et al.*, 2021).

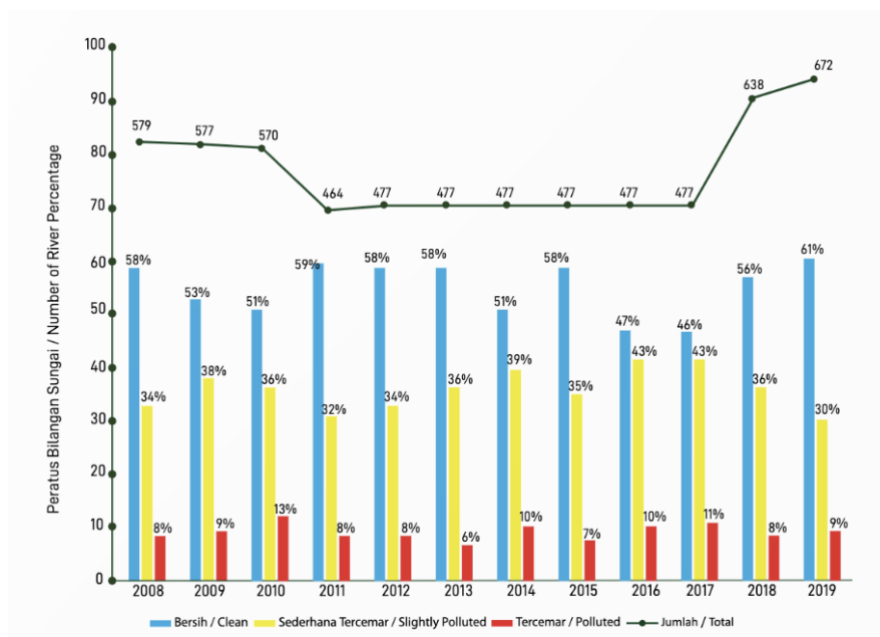


Figure 1.3: River water quality trend in Malaysia from year 2008-2019 (Rani *et al.*, 2021).

Common wastewater treatment plants (WWTPs) are difficult to completely remove this kind of organic dye pollutants (e.g. MB) particularly in ppm level. These azo and reactive dyes are electron-deficient in nature, which makes them less susceptible to oxidative catabolism. Moreover, the MB dye present in wastewater has high stability, complex composition, anti-biodegradable properties make it difficult to be degraded. When the MB is difficult to be degraded, it will have chance to be intake by human and animals through tap water and other water source.

Therefore, advanced oxidation process (AOPs) is introduced as the complementary technique to degrade the non-biodegradable and highly stable organic compounds. AOPs is generally a degradation technology that uses the hydroxyl radicals which is the ultimate oxidant to degrade organic contaminants in wastewater. AOPs can be combined with ozone ( $O_3$ ) (Rekhate and Srivastava, 2020), catalyst (Buthiyappan, Abdul Aziz and Wan Daud, 2016), or ultraviolet (UV) irradiation (Guo, Wu and Fang, 2019) to provide a strong treatment of wastewater. This technology utilizes the in-situ production of hydroxyl radicals and sulphate radicals which can effectively remove organic pollutants.

There are two types of AOPs, which are homogeneous and heterogeneous AOPs. Both processes can be done with or without the irradiation of ultrasound energy and ultraviolet energy. The irradiation of the solution with these irradiation sources will only speed up the rate of production of hydroxyl species which will result in increasing the overall efficiency of AOPs. For example, homogeneous AOPs which uses UV radiation (in the presence of  $O_3$  or  $H_2O_2$ ) to degrade compounds that will absorb UV radiation within the corresponding range of spectrum. Heterogeneous AOPs is a photochemical oxidation process that uses catalyst for compounds' degradation. "Heterogeneous" refers to there is presence of contaminants which is the catalyst (solid phase) in the solution



(aqueous phase). The presence of the catalyst will accelerate the AOPs due to the presence of electron-hole pairs and the photogenerated electrons and holes will result in oxidation and reduction processes respectively. Figure 1.4 shows the major types of AOPs which basically split into homogeneous and heterogeneous AOPs (Mayyahi and Al-asadi, 2018). In summary, heterogeneous AOPs will be faster than homogeneous AOPs due to the presence of catalyst. Moreover,  $\text{TiO}_2$  has a higher oxidation power as compared to other oxidizing species which makes  $\text{TiO}_2$  system has better efficiency.  $\text{H}_2\text{O}_2$  system has poor UV light absorption characteristics (wasting most of the light input) and Electron-Fenton reaction required low pH to keep the iron in solution (increases maintenance and operation cost), which makes  $\text{UV}/\text{O}_2/\text{TiO}_2$  a better system (Krishnan *et al.*, 2017).

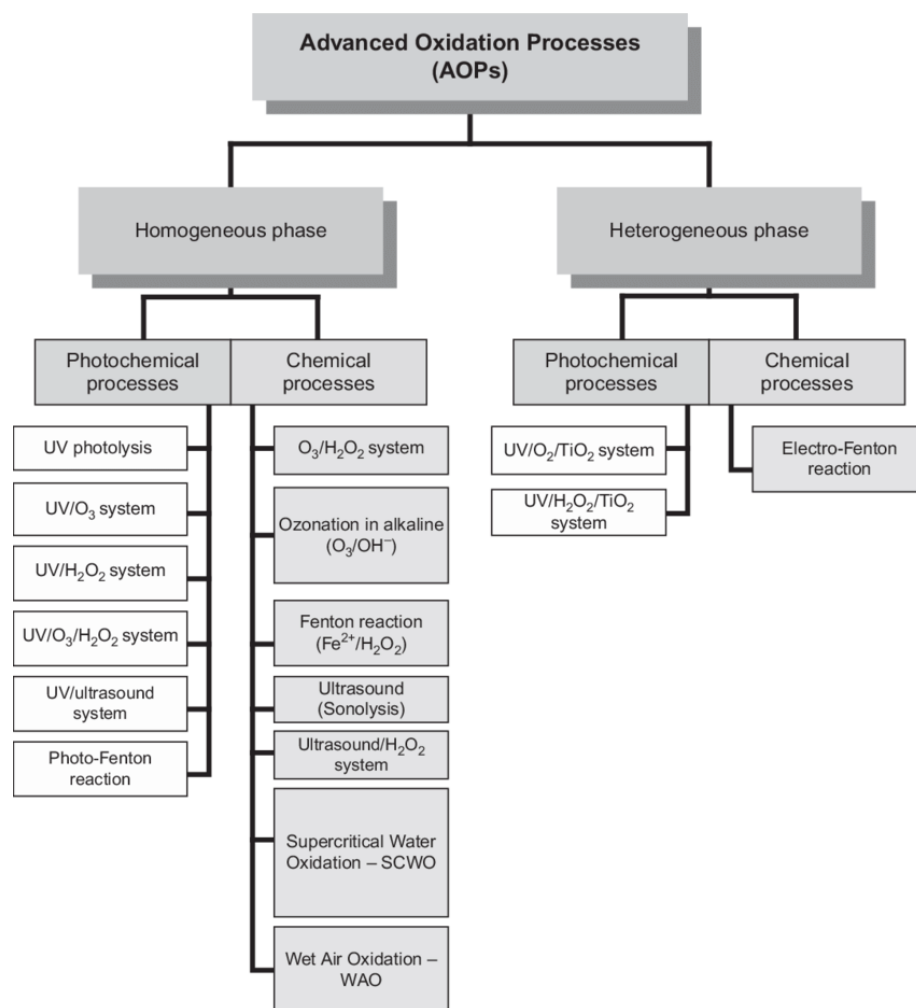
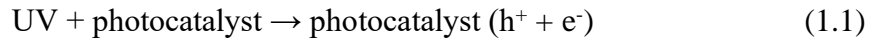


Figure 1.4: Major types of Advanced Oxidation Processes (Biń and Sobera-Madej, 2012)

In this research project, heterogeneous AOPs or photocatalytic oxidation will be the main focus as titanium dioxide ( $\text{TiO}_2$ ) is the catalyst that would be used to degrade the organic dye i.e. MB (Ghime and Ghosh, 2020).  $\text{TiO}_2$  is the most widely used photocatalyst for the photocatalytic activity (PCA) as  $\text{TiO}_2$  is stable, inexpensive, high photo-activity and non-toxic. AOPs processes is getting more important in wastewater treatment as this process able to fully mineralization the pollutants under ambient temperature and pressure than other degradation processes. Moreover, photocatalytic process only used sunlight or UV light which could save a lot of operational cost especially for operations that are large-scale.

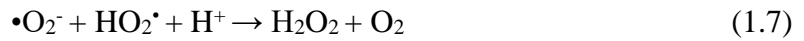
Photocatalytic reactions occur when photocatalysts such as  $\text{TiO}_2$  are irradiated by appropriate light sources that larger than its band gap. When the photocatalyst such as  $\text{TiO}_2$  absorb light that greater than its bandgap energy, it will excite electrons from valance band to its conduction band. This will produce positively charged holes in the valence band and electrons in the conduction band. Some of these charge carriers will be lost on the way diffuse to the surface of photocatalysts, but some of them will be managed to reach the surface of photocatalysts. Then, oxidation-reduction reaction will take place at the surface of the photocatalysts. Subsequently, the photo-generated electrons can produce super oxide anion free radicals ( $\bullet\text{O}_2^-$ ) when react with dissolved oxygen and generate hydroxyl free radicals ( $\bullet\text{OH}$ ) when the holes react with water molecules as shown in Equation. (1.1) – (1.8) (Saharan *et al.*, 2014). These reactive species are capable of decomposing the molecular species that contact with the  $\text{TiO}_2$  into less harmful by-product. Nevertheless,  $\text{TiO}_2$  only actives under the irradiation of UV light but not so effective under visible light due to its wide band gap (3.0 eV for rutile phase, 3.2 eV for anatase phase). It also suffers from rapid recombination of photogenerated electron-hole pairs (Sreekantan, Saharudin and Wei, 2011).



For the reactions that involve holes:



For the reactions that involve electrons:



Hydroxyl radicals have high oxidation potential which can oxidize organic pollutants into smaller organic molecules. Figure 1.5 illustrates the general photocatalytic degradation mechanism of Volatile Organic Compounds (VOC) performed by  $\text{TiO}_2$  as discussed above.

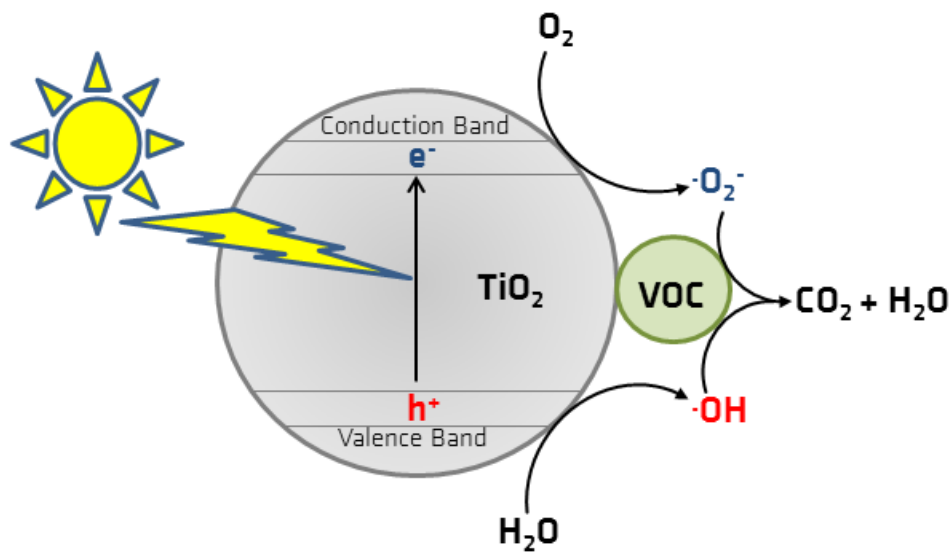


Figure 1.5: Photocatalytic degradation mechanism (Mull, Möhlmann and Wilke, 2017)

## 1.2 Problem statement

(1) Long synthesis duration, high equipment, and operational cost

TiO<sub>2</sub> is a widely used photocatalyst for PCA (Atta ul Haq; Muhammad Saeed; Samreen Gul Khan; Muhammad Ibrahim, 2021). There are various methods that can be used to synthesize TiO<sub>2</sub> particles such as hydrothermal method (Sun, Qadir and Jeong, 2014a), template-assisted method (Date *et al.*, 2020), sol-gel method (Marien *et al.*, 2017), electrochemical anodizing method (Bhattacharyya *et al.*, 2016), microwave-assisted method (May-Masnou *et al.*, 2018), and chemical vapour deposition method (Zhang and Li, 2018). Hydrothermal and sol-gel method are commonly used to produce TiO<sub>2</sub> particles as these methods are easy to obtain the desired nanostructure size and morphology. However, the major problems of these methods are long synthesis duration as summarized in Table 1.1. It can take more than 24 hours for the heating in the furnace and after heating it needs to be washed and dry for another 24 hours, thus it is very time-consuming (Sun, Qadir and Jeong, 2014b). Moreover, for sol-gel method that uses autoclave and Chemical Vapour Deposition (CVD) method that uses vacuum system, will require high equipment cost that might not be suitable for mass production.

Direct Heating technique is a simple 1 step process with ultra-rapid growth process which takes less than 1 hour. Therefore, it can save the processing time. Furthermore, this technique will be energy saving as well due to the alternating current (AC) electrical current is introduced directly to the wires, thus it is an in-situ heating process, and the heat is uniformly generated from the substrate to the solution. Based on Table 1.1, Direct Heating technique takes less than 1 hour for the synthesis of TiO<sub>2</sub> nanoparticles while hydrothermal takes more than 61 hours and sol-gel method takes more than 12 hours. Moreover, Direct Heating technique only used RM 710 for equipment cost which is cheaper than hydrothermal method (RM 16789.45) and sol-gel

method (RM 19330.67). Moreover, direct heating technique only uses 0.06 kWh per run which led to (RM 0.01332) energy consumption cost per run which is cheaper than hydrothermal method (RM 13.26672) and sol-gel method (RM 4.8063). Detail calculation of the costs and power consumption will be in Appendix A.

Table 1.1: A comparison of synthesis duration, equipment cost, energy used and operational cost for the synthesis of TiO<sub>2</sub> particles

Methods	Synthesis Duration (hour)	Equipment Cost (RM)	Energy used (kWh)	Energy Consumption Cost (RM)
Hydrothermal	> 61	16789.45	59.76	RM 13.2667
Sol-gel	> 12	19330.67	21.65	RM 4.8063
Direct Heating Technique	< 1	710.00	0.06	RM 0.0133

(2) Deterioration of photodegradation efficiency over time and generation of secondary pollutants

For most photocatalytic application, TiO<sub>2</sub> was used mainly in particle form. It tends to be carried away by running water during the treatment of wastewater. Therefore, the photocatalytic performance will deteriorate over time. The washed away TiO<sub>2</sub> particles become secondary pollutants. Besides, TiO<sub>2</sub> particles may undergo aggregation due to the instability of its nanosized. This will reduce the light incidence on the active centres that lead to the deterioration of its photodegradation efficiency. Therefore, the TiO<sub>2</sub> particles need to be grown on supporting substrate to minimize this problem to be happened (Dong et al., 2015).

### **1.3 Research objectives**

1. To synthesize TiO<sub>2</sub> particles on Kanthal wire by using Direct Heating technique with different heating duration and heating power.
2. To measure the structural, optical and photocatalytic performances of TiO<sub>2</sub> particles that grown on Kanthal wire and TiO<sub>2</sub> particles by products.

### **1.4 Scope of study**

In this research project, TiO<sub>2</sub> particles were grown on the Kanthal coil by using Direct Heating technique. Process optimization was carried out by systematic studied two synthesis parameters, which were the effect of heating duration and heating power. The TiO<sub>2</sub> particles that grown on Kanthal coil and by-product i.e. TiO<sub>2</sub> particles that collected at the bottom of beaker, were sent for various characterizations. X-ray Powder Diffraction (XRD) was used to study the crystallinity and crystal orientation of the products. Field emission scanning electron microscopy (FESEM) was used to study the surface morphologies of the product. Transmission electron microscopy (TEM) was used for direct imaging of lattice structure and determining the morphology of the product at nanoscale. Fourier Transformed Infrared (FTIR) spectroscopy was used to identifies the presence of organic and inorganic compounds in the sample. Ultraviolet–visible (UV-Vis) spectroscopy was used to record the optical transmission spectra of the product. The degradation efficiency of MB solution by TiO<sub>2</sub> was studied in this project. Scavenger test with various reagent species was carried out with the TiO<sub>2</sub> by product to identify the main reactive species that involve in the degradation of MB solution. Lastly, TiO<sub>2</sub> by product produced by Direct Heating technique was compared with the commercial TiO<sub>2</sub> in terms of photodegradation efficiency in the degradation of MB solution.

## 1.5 Thesis outline

This thesis consists of 5 chapters.

**Chapter 1** discuss about the background of study in this project, problem statement, research objectives and scope of study.

**Chapter 2** presents the literature review of TiO<sub>2</sub> and its application, and also the synthesis route of TiO<sub>2</sub> nanostructure that includes hydrothermal method, template-assisted method, sol-gel method, electrochemical anodization, microwave-assisted method, chemical vapour deposition, and Direct Heating technique. Moreover, the advantages and disadvantages of these methods will also be summarized in a table. Lastly, MB solution and its degradation mechanism by TiO<sub>2</sub> will be discussed in this chapter.

**Chapter 3** will firstly show the overall project flow chart and then introduce the materials and equipment used in this project. The synthesis and characterization of the TiO<sub>2</sub> particles grown on Kanthal wire by Direct Heating technique also will be discussed. This includes the experimental procedure and experimental design. Furthermore, the procedure of photocatalytic oxidation of MB solution by TiO<sub>2</sub> particles and TiO<sub>2</sub> by-products will be presented.

**Chapter 4** discusses on the results obtained from various characterization techniques on the product and will support the hypothesis and arguments with theoretical body of knowledge.

**Chapter 5** concludes all key findings of this projects and recommends potential research works for future study.

## CHAPTER 2 LITERATURE REVIEW

### 2.1 Introduction

In this chapter, Titanium Dioxide ( $\text{TiO}_2$ ) and its applications will be discussed. There are many synthesis methods for  $\text{TiO}_2$  nanomaterials for examples hydrothermal method, template-assisted method, sol-gel method, electrochemical anodization, microwave-assisted method, CVD, and most importantly direct heating method. The working principles, strengths and weaknesses of these synthesis methods will be discussed, compared, and summarized into a table. Lastly, the photocatalytic oxidation of MB solution by  $\text{TiO}_2$  nanomaterials will also be presented.

### 2.2 Titanium Dioxide ( $\text{TiO}_2$ )

$\text{TiO}_2$  could be found in nature in different forms, for examples anatase, rutile, and brookite as shown in Figure 2.1. Brookite phase of the titanium dioxide is metastable. It is not suitable to be used in photocatalytic applications. Therefore, rutile and anatase phase of the titanium dioxide will be used for photocatalytic activity as these phases are thermodynamically stable phases. Anatase phase has a better photocatalytic performance than rutile phase due to its larger band gap (3.2 eV) than rutile phase (3.0 eV), as this raises the valence band to higher energy levels relative to redox potentials of adsorbed molecules which increases the oxidation power of electrons and facilitates electron transfer from the  $\text{TiO}_2$  to adsorbed molecules (Luttrell *et al.*, 2015a). Brookite has been rarely used and studied because it has a complicated structure and most difficult to synthesis in pure form, so its electronic bandgap and optical property are still under deliberation. However, based on the study of Johari *et al.* (2021), the team had successfully produced brookite film with the bandgap of 3.37 eV via green sol-gel route. Studies have shown that mixed phase between rutile and anatase phase of titanium dioxide



had a higher photocatalytic performance. This was because the movement of photoinduced electrons from rutile to anatase phase of titanium dioxide pro-longed the recombination of positive holes and electrons, thus greatly improved the photocatalytic performance (Haq *et al.*, 2021).

Titanium ( $\text{Ti}^{4+}$ ) atoms are coordinated to six oxygen ( $\text{O}^{2-}$ ) atoms, forming “ $\text{TiO}_6$ ” octahedra, and all forms of  $\text{TiO}_2$  are formed by chains of distorted  $\text{TiO}_6$  octahedra. Nevertheless, both rutile and anatase  $\text{TiO}_2$  have the tetragonal crystal structure while brookite has the orthorhombic crystal structure. Unit cell of tetragonal anatase  $\text{TiO}_2$  contain four units (12 atoms), while the unit cell for tetragonal rutile  $\text{TiO}_2$  is two units (6 atoms), and the unit cell for orthorhombic brookite  $\text{TiO}_2$  is eight units (24 atoms). The formation of  $\text{TiO}_2$  phase is critical in determining the properties of the materials. Generally, the initial crystalline  $\text{TiO}_2$  phase will be anatase due to it is easier for the  $\text{TiO}_6$  octahedra in arranging into long-range ordered anatase structure and a less-constrained molecular structure. Rutile will be obtained through calcination, and the transformation of anatase to rutile is reconstructive and irreversible as the transformation involves bonds breaking and reforming. Rutile phase is the most thermally stable phase among the three polymorphs and the phase transformation usually occurs at 600 °C when calcined in air.

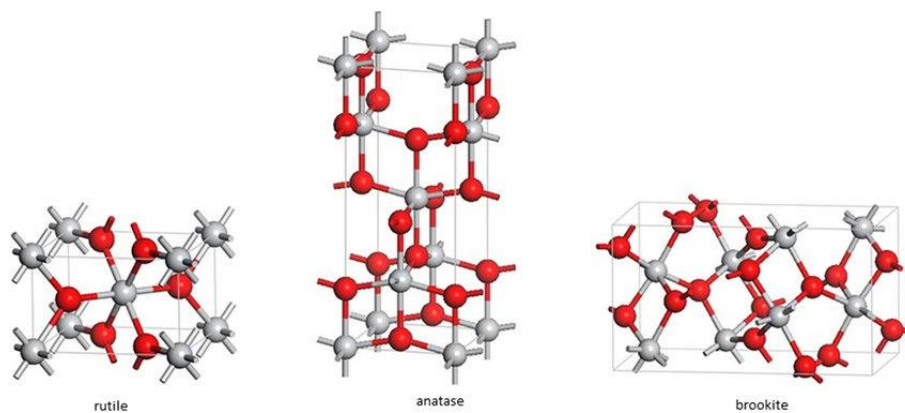


Figure 2.1: Crystal structure of crystalline forms of rutile, anatase and brookite  $\text{TiO}_2$  NPs (Baranowska-Wójcik *et al.*, 2020)

According to the studies of (Haq *et al.*, 2021), anatase TiO<sub>2</sub> has the highest photocatalytic performance due to wider band gap, indirect band gap, lower electron-hole recombination rate, and higher charge carrier mobility. Thus, it is preferred for the degradation of MB solution in this project. Besides, photocatalytic activity of TiO<sub>2</sub> will be limited by the rapid recombination of the photogenerated electron-hole pairs. This is because the recombination of the charge carriers will reduce the production of hydroxyl radicals ( $\bullet\text{OH}$ ) and other oxidants like superoxide radical anion ( $\text{O}_2^{\bullet-}$ ) which lead to degradation of the photocatalytic activity. Therefore, the presence of mixed phases (rutile phase + anatase phase) can enhance the photocatalytic performance due to the movement of photoinduced electrons from rutile to anatase phase which can minimize the recombination of positive holes and electrons.

### **2.2.1 TiO<sub>2</sub> for photocatalyst application**

TiO<sub>2</sub> is also widely used as photocatalysts for organic and inorganic pollutants removal (Khalilova, Hasanova and Aliyev, 2018; Azzaz *et al.*, 2021), inactivation of bacterial and fungal (Mitoraj *et al.*, 2007), water splitting for oxygen and hydrogen generation (Eidsvåg *et al.*, 2021) and self-cleaning substrates (Yadav and Kim, 2017). The photocatalytic performances of photocatalysts depend on the ability of catalyst to create electron-hole pairs which subsequently to generate free radicals that are able to undergo secondary reactions. Photocatalytic technology that uses semiconductors can convert solar energy into other chemical energy. This helps to address the energy and environmental problem that rises due to the depletion of fossil fuel and rising amount of greenhouse gases. Metal oxide semiconductors such as Zinc oxide (ZnO) (Khalafi, Buazar and Ghanemi, 2019), Magnesium oxide (MgO) (Algethami *et al.*, 2021), Zirconium oxide (ZrO<sub>2</sub>) (Długosz, Szostak and Banach, 2020), and TiO<sub>2</sub> (Nasikhudin *et*

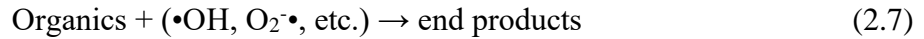
*al.*, 2018) are the materials that can be used in PCA. TiO<sub>2</sub> is the most widely used photocatalyst for the PCA as it is chemically stable, inexpensive, high photoactivity and non-toxic. However, TiO<sub>2</sub> only activates under the irradiation of UV light but not so effective under visible light due to its wide band gap (3.0 eV for rutile phase, 3.2 eV for anatase phase). It also suffers from rapid recombination of photogenerated electron-hole pairs (Nasikhudin *et al.*, 2018).

The photocatalytic mechanism of TiO<sub>2</sub> for organic pollutants removal is described below. When TiO<sub>2</sub> is irradiated by optical light source with energy that greater than its band gap energy ( $E_g$ ) of the TiO<sub>2</sub> (for example  $h\nu > E_g = 3.2$  eV in the case of anatase TiO<sub>2</sub>), it will generate holes ( $h_{vb}^+$ ) and electrons ( $e_{cb}^-$ ) in its valence band and conduction band respectively according to Equation (2.1):



The  $h_{vb}^+$  and  $e_{cb}^-$  will make their ways to to surface of the TiO<sub>2</sub> where they will react with the organic species (in this project is MB solution) which adsorbed onto the catalyst surface, or they might recombine to liberate heat. The  $h_{vb}^+$  and  $e_{cb}^-$  will react with the organics to form end products like water and carbon dioxide. Besides, these charge carriers will react with water, hydroxide ions and oxygen to produce  $\bullet\text{OH}$  and other oxidants like  $\text{O}_2\bullet$  which can further mineralize the organic compounds (MB solution) to end products. The reactions are summarized as below (Yang, Yu and Ray, 2008):





In summary, TiO<sub>2</sub> nanomaterials have diverse applications. Particularly, it is well known as effective photocatalyst to break down almost any organic compound when exposed to sunlight. It has wider band gap, non-toxic to environment and chemically stable. Thus, TiO<sub>2</sub> is extremely good to be used as photocatalyst. In this project, MB solution was selected as targeted organic compound because it has high stability, complex composition, anti-biodegradable properties make it difficult to be degraded. High concentration of MB intake by human will cause nausea, abdominal and chest pain, dizziness, headache, confusion, and methaemoglobinaemia. Therefore, MB solution needs to be removed, in this case, by TiO<sub>2</sub> photocatalyst.

### **2.3 Synthesis route of TiO<sub>2</sub> nanomaterials**

There are various methods that can be used to synthesize TiO<sub>2</sub> nanomaterials such as hydrothermal method (Sun, Qadir and Jeong, 2014a), template-assisted method (Date *et al.*, 2020), sol-gel method (Marien *et al.*, 2017), electrochemical anodizing method (Bhattacharyya *et al.*, 2016), microwave-assisted method (May-Masnou *et al.*, 2018), chemical vapour deposition (Zhang and Li, 2018) and direct heating method (Lee *et al.*, 2017). The working principle of these synthesis methods, as well as their strengths and weaknesses will be discussed in this sub-section.

#### **2.3.1 Hydrothermal method**

Hydrothermal method is a process of crystallizing a substance with high temperature and high vapour pressure using an aqueous solution of the material. Hydrothermal process is used for the crystal growth of substance particularly that are insoluble in customary temperature (100°C) and pressure (<1 atm). This process is carried

out or conducted in a specially sealed container or high-pressure stainless-steel autoclave under subcritical or supercritical conditions of solvent as illustrated as Figure 2.2. Then, the temperature gradient is maintained between the opposite ends of the growth chamber. Lastly, the nutrient solute dissolves at the hotter end while the desired seed crystal will be deposited on the cooler end (Kafle, 2020).

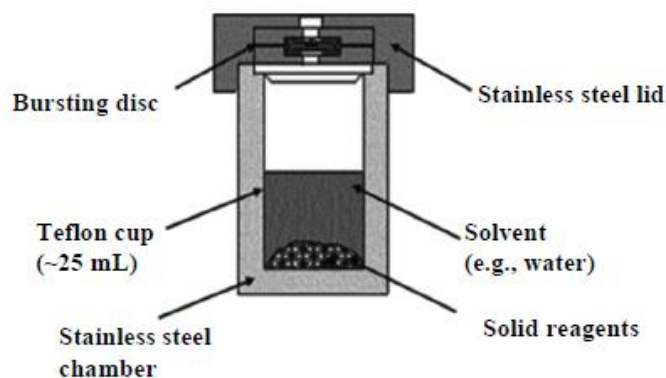


Figure 2.2: Teflon lined stainless steel autoclaves with inner components (Kafle, 2020)

By using hydrothermal synthesis, many types of nanomaterials have been successfully synthesized. This is because hydrothermal synthesis can generate nanomaterials which are not stable at high temperature. High vapour pressure can be generated with minimum loss of materials, and well controlled composition of nanomaterials can be produced (Gan *et al.*, 2020). Rehan, Lai and Kale (2011) had successfully synthesized TiO<sub>2</sub> nanoparticles by hydrothermal synthesis. The TiO<sub>2</sub> nanoparticles were produced from an acid (HNO<sub>3</sub>) and an alkaline (tetrabutylammonium hydroxide; TBA) peptized gel by hydrothermal treatment at 210 °C and 270 °C, respectively as shown in Figure 2.3. The Energy dispersive X-ray diffraction (EDXRD) results showed that pure TiO<sub>2</sub> rutile phase nanoparticles were crystallized from the acid peptized gel while TiO<sub>2</sub> anatase phase nanoparticles were crystallized from the alkaline peptized gel. TEM result showed that the anatase phase nanoparticles were more

homogeneous in size while rutile phase nanoparticles exhibited bimodal size and morphology distribution due to Ostwald ripening effect during synthesis.

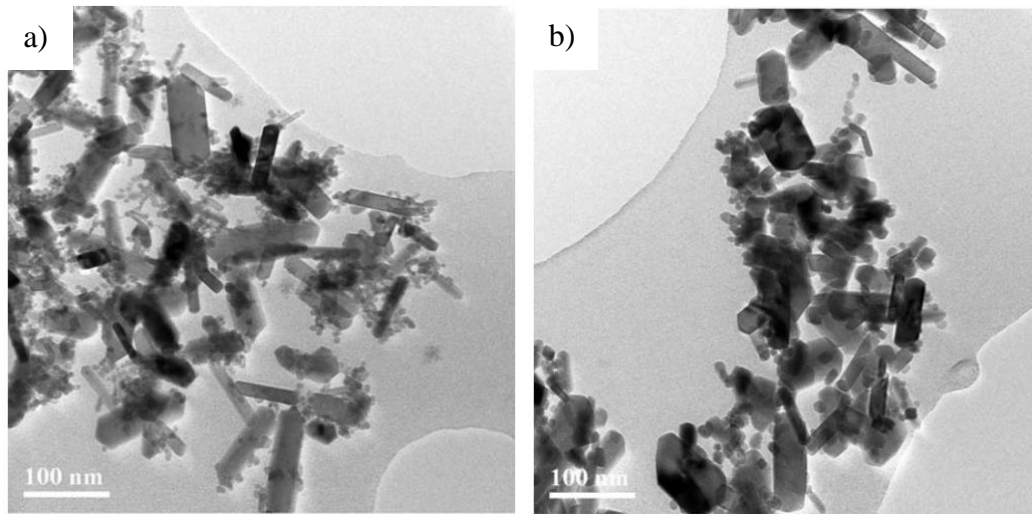


Figure 2.3: TEM image of TiO<sub>2</sub> nanoparticles after hydrothermal treatment of HNO<sub>3</sub> peptized gel at (a) 210 °C and (b) 270 °C (Rehan, Lai and Kale, 2011)

### 2.3.2 Template-assisted method

Template-assisted method or template-assisted electrodeposition is an important technique to synthesize metallic nanomaterials with controlled or desired shape and size. It used a nano porous material as the mould and the desired nanotube material will be coated or deposited on the walls of the mould. Then, the template will need to be dissolved in order to get the nanotubes or nanorods. There are negative and positive template, negative template-based synthesis is the material of interest is coated on the inner walls while positive template-based synthesis is the material of interest is coated on the outer walls. Examples of templates are anodized alumina membranes (AAO) (Gujela, Gujela and Gayatri, 2016), radiation track etched polymer membranes (Starosta, 2017), carbon nanotubes (Li *et al.*, 2015). Figure 2.4 shows the SEM image of commercial AAO membrane (top view) (Pradel and Fukata, 2022).

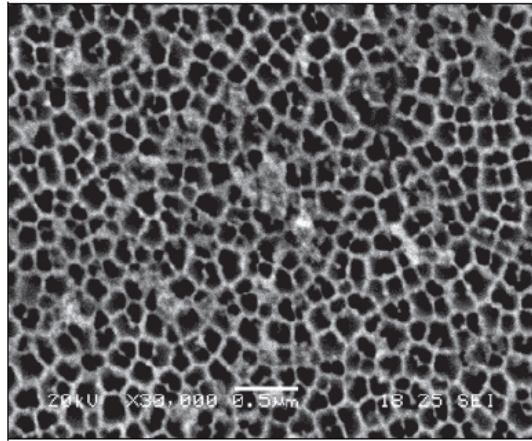


Figure 2.4: SEM image of commercial AAO membrane (top view) (Pradel and Fukata, 2022)

Figure 2.5 shows the working principle of AAO template-assisted electrodeposition method (Pradel and Fukata, 2022). Generally, the process of template-assisted method starts by attaching the template onto the cathode and then brought into contact or dip into the deposition solution or precursor solution. Then, the anode will be placed in the deposition solution that is parallel to the cathode. When the electric field is applied, cation will diffuse towards the cathode, resulting in the growing of nanotube/nanorod/nanowire inside the template. Lastly, this template will be dissolved in alkaline solution and the desired nanomaterials are obtained.

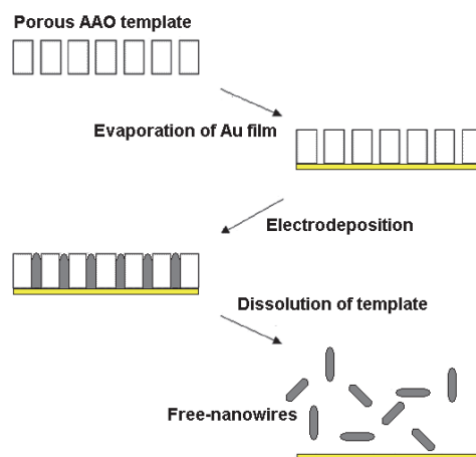


Figure 2.5: Working principle of AAO template-assisted electrodeposition method (Pradel and Fukata, 2022)

Lai et al. (2010) selectively deposited cadmium sulfide (CdS) nanospheres on TiO<sub>2</sub> nanotubes layers to form uniformly coupled CdS/TiO<sub>2</sub> semiconductor heterojunction micro-pattern by template-assisted electrodeposition method. The CdS/TiO<sub>2</sub> showed a greatly enhanced photocurrent response in both UV and visible light range. In another study by Date et al. (2020), the team had successfully synthesized three-dimensional (3D) CuO/TiO<sub>2</sub> hybrid heterostructure nanorod arrays (NRs) by using AAO template-assisted electrodeposition method. It is followed by annealing. The anatase phase of TiO<sub>2</sub> formed when it was annealed at 400 °C for 12 hours but rutile phase formed when it was annealed at 600 °C for 12 hours. It was then used as photocatalyst to degrade dye. Nevertheless, the presence of rutile phase of TiO<sub>2</sub> decreased the photocatalytic performance.

### **2.3.3 Sol-gel method**

Sol-gel method is a wet-chemical technique which convert a precursor solution to an inorganic solid through polymerization reactions that induced by water. Sol is meant by the dispersion of colloidal particles in a liquid by hydrolysis while gel is formed by the condensation process. This method is good in synthesis and preparation of inorganic and organic-inorganic hybrid nanomaterials as it uses low processing temperatures (<100°C) and molecular level composition homogeneity.

This method starts with the molecular precursor that usually metal alkoxide. This precursor will be dissolved in water or alcohol in order to form sol. The sol is converted to gel via hydrolysis/alcoholysis by heating and stirring. The gel obtained will be wet or damped. It should be dried using appropriate method, for examples supercritical drying, thermal drying, or freeze drying, to get the desired properties. Lastly, the gel produced



after drying stage will be aerogel or xerogel or cryogel. It is then calcined to become powder form. Figure 2.6 shows the schematic diagram of different stages of sol-gel process. This method is a conventional and industrial method to produce nanoparticles with different chemical composition. Moreover, sol-gel process is a bottom-up synthesis method in which the final products are formed by performing a number of irreversible chemical reactions (Bokov *et al.*, 2021).

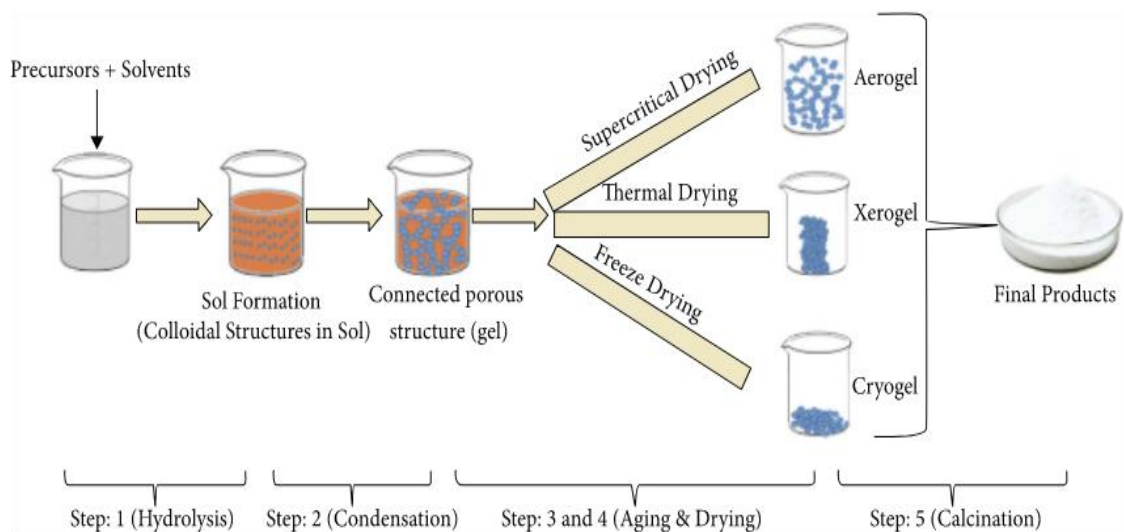


Figure 2.6: Schematic diagram of different stages in sol-gel process (Bokov *et al.*, 2021)

Marien *et al.* (2017) had successfully synthesized  $\text{TiO}_2$  nanoparticles by modifying an acid-catalysed sol-gel synthesis with Pluronic PI23. The process started with mixing titanium tetra-isopropoxide (TTIP) and anhydrous ethanol in the meantime (Solution A). Solution B was prepared by mixing anhydrous ethanol with distilled water and acetic acid. Then, this mixture was added dropwise into solution A to form a clear transparent sol. The mixed solution was left for few hours in order to form gel. Lastly, the gel was dried and calcined to get the anatase  $\text{TiO}_2$  nanoparticles. Dubey, Krishnamurthy and Singh (2019) had successfully synthesized  $\text{TiO}_2$  nanoparticles by the sol-gel process. Figure 2.7 (a-c) show that the  $\text{TiO}_2$  nanoparticles formed were

homogeneous distributed with spherical shape while Figure 2.7 (d) shows that polycrystalline anatase TiO<sub>2</sub> nanoparticles were formed by sol-gel method.

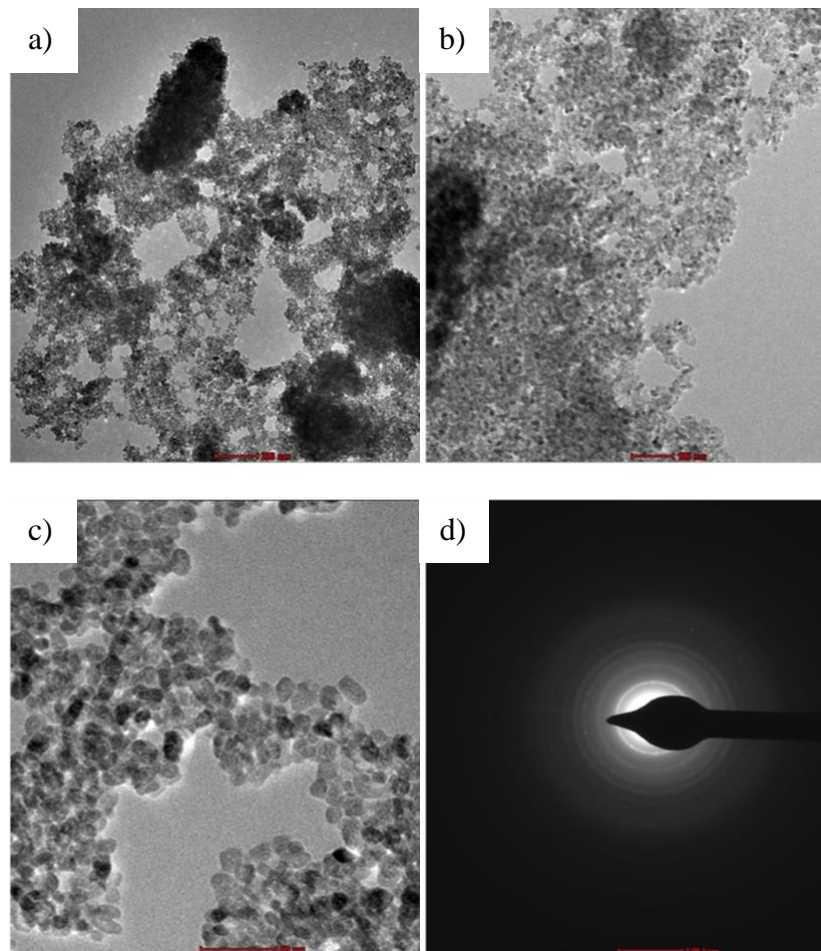


Figure 2.7: TEM micrographs of TiO<sub>2</sub> nanoparticles formed by sol-gel process at resolution (a) 200 nm (b) 100 nm (c) 50 nm (d) SAED pattern (Dubey, Krishnamurthy and Singh, 2019)

### 2.3.4 Electrochemical anodization

Electrochemical anodization is an electrolytic process to grow oxide layer on the metal surface. During this process, the metal to be treated (titanium) will be the anode electrode of the electric circuit while cathode will be any electronic conductor like platinum or copper that will not react in the anodization bath. Electrolyte will be chosen to its higher growing rate of the oxide compared to its dissolution rate or by the insolubility with the anodized metal. During the anodization, metal at positive terminal

will withdraws electrons which allows the ions on the metal surface to react with water in electrolyte to form a dense oxide later. Then, the electrons will return to the electrolyte and react with hydrogen gas to liberate hydrogen gas (Nyamukamba *et al.*, 2018).

For instances, Bhattacharyya *et al.* (2016) had successfully synthesized titania nanotubes by electrochemical anodization of titanium foils. The titanium foils were cut into coupons and cleaned under sonification. The titanium coupons were attached to the anode and platinum mesh was used as cathode. It was noted that the coupons were anodized in a fluorinated ethylene glycol solution (0.5 wt%  $\text{NH}_4\text{F}$  + 2 wt%  $\text{H}_2\text{O}$ ) for 1 hour in a Teflon beaker under magnetic stirring at 60 rpm. The other sides of the coupon were covered by masking tape to ensure the growth of titanium nanotube only on 1 side of the coupon. Lastly, the anodized coupons were calcined in the furnace to get the titanium nanotube array. Figure 2.8 shows the experiment setup of electrochemical anodization for the synthesis of titania nanotube array (TNA) (Bhattacharyya *et al.*, 2016). Figure 2.9 shows the SEM micrograph of  $\text{TiO}_2$  nanotube top view and side view synthesized by electrochemical anodization (Bhattacharyya *et al.*, 2016).

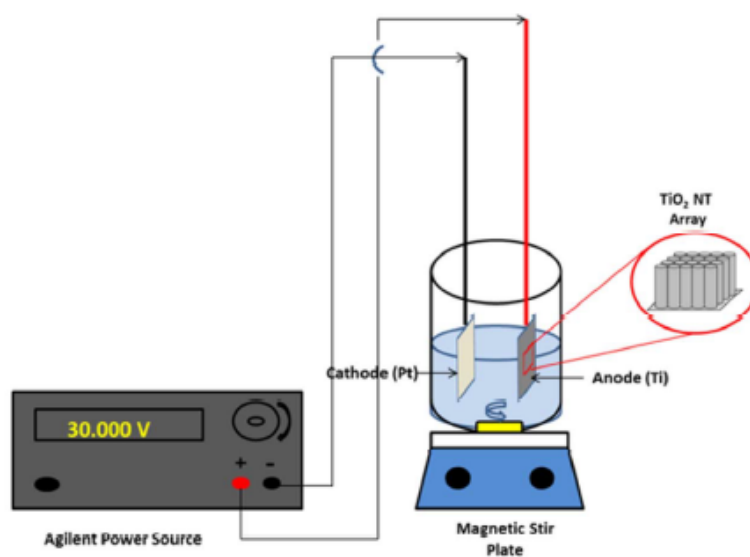


Figure 2.8: Experiment setup of electrochemical anodization for synthesis of titania nanotube array (TNA) (Bhattacharyya *et al.*, 2016)